OPTICS

Nanoscale Lamb wave–driven motors in nonliquid environments

Jinsheng Lu[1], Qiang Li[1], Cheng-Wei Qiu[2], Yu Hong[1], Pintu Ghosh[1], Min Qiu[1,3,4]*

Achieving light-driven motions in nonliquid environments presents formidable challenges, because microsized objects experience strong dry adhesion and intend to be stuck to contact surfaces with great tenacity. Here, in air and vacuum, we show rotary locomotion of a micrometer-sized metal plate with ~30 nm thickness, revolving around a microfiber. This motor is powered by pulsed light guided into the fiber as a coordinated consequence of an optically excited Lamb wave on the plate and favorable configuration of plate-fiber geometry. The motor, actuated by designed light pulses, crawls stepwise with subnanometer locomotion resolution. Furthermore, we can control the rotation velocity and step resolution by varying the repetition rate and pulse power, respectively. A light-actuated micromirror scanning with 0.001° resolution is then demonstrated on the basis of this motor. It offers unprecedented application potential for integrated micro-opto-electromechanical systems, outer-space all-optical precision mechanics and controls, and laser scanning for miniature lidar systems.

INTRODUCTION

Rotation in micro/nanoscale provides extensive applications in mechanical actuation (*1*, *2*), cargo delivery (*3*, *4*), and biomolecule manipulation (*5*, *6*). Light can be used to induce a mechanical rotation remotely, instantly, and precisely (*7*–*13*). Light-driven rotation has been well demonstrated by transferring linear (*8*, *9*) or angular (*10*–*13*) momentum to microsized objects in liquid environments. It is easy to assume that these optical manipulation phenomena will be naturally present in nonliquid environments. However, dominant adhesion in nonliquid environments rules out such notions. Adhesion force for a usual micrometer-sized object could easily reach a high value (~μN) (*14*, *15*), which exceeds both its gravity (~pN) and the typical value of optical force (~pN) in experiments (*16*) by a factor of $>10^6$. Adhesion seriously impedes the operation of rotary motors actuated by this kind of momentum transferring, and thus, liquid is widely used to erase the unwanted impact of adhesion. Deviating from this long-held view, we report a light-actuated motor in which the adhesion counterintuitively becomes the key enabler for the rotation, with synergetic assistance from the Lamb wave (which is generated due to thermoelastic expansion by plasmonic heating of the absorbed pulsed light) and geometrical configuration.

RESULTS

The experimental setup is shown in Fig. 1A. A uniformly fine-drawn optical microfiber is suspended in air or vacuum, where a gold plate is placed on it by using a probe (fig. S1). This plate-microfiber system can be seen in the scanning electron microscopy (SEM) image (Fig. 1B). We attempted to switch a continuous wave (CW) laser on/off, and a subtly weak azimuthal movement of the gold plate was spotted at the instantaneous ON/OFF moments. This movement is due to the expansion/contraction of the gold plate (*17*). This accidental effect triggers us to deliver a pulsed supercontinuum light into the microfiber, thereby enabling almost stably continuous azimuthal rotation. The gold plate (i.e., the motor) starts to revolve around the microfiber once the light pulses are guided into the microfiber.

The gold plate is tightly attached on the surface of the microfiber due to dry adhesion force, which is the well-known van der Waals force. The gold plate is a single crystal with an atomic smooth surface, and the surface of the fabricated microfiber is also rather smooth. Thus, the separation between the two touched surfaces of the gold plate and the microfiber is so small that the van der Waals force becomes dominant. As the van der Waals force is nondirectional, it can work in two orthogonal directions. In the radial direction (i.e., perpendicular to the contact surface), this adhesion force works as an attractive centripetal force to enable the gold plate to tightly touch the circular outer surface of the microfiber. In the azimuthal direction (parallel to the contact surface), this adhesion force acts as a friction force to prevent the gold plate from sliding on the surface of the microfiber. This adhesion force is measured to be 6.9 μN (section S1), which is six orders of magnitude higher than the gravity of the gold plate (1.8 pN). The gravity of the gold plate thus takes a negligible effect during the rotation. We also conducted this experiment in liquid, where the adhesion force becomes rather small. In this case, the gold plate leaves the microfiber and does not rotate around the microfiber anymore. This proves that the adhesion force is indispensable for this rotation.

The optical microscope images (Fig. 1C) sequentially demonstrate the rotation of the motor in air (see movie S1). The motor rotates at ~1.4 Hz anticlockwise (viewed in the direction of the light propagation). The rotation is due to the asymmetric placement of the gold plate on the microfiber, and the rotation direction is dependent on the initial relative location of the plate on the microfiber. The gold plate rotates anticlockwise (Fig. 1C) in the "right-shifted" case (that is, the plate is placed on the top of the microfiber and the center of the plate is shifted toward the right half of the microfiber). It rotates clockwise in the "left-shifted" case (see Fig. 1D for comparison). If the gold plate is placed on the microfiber in a symmetric configuration, it hardly rotates. Note that the rotation direction is determined by the different asymmetries (i.e., right-shifted and left-shifted) and has nothing to do with the gravity of the gold plate (as mentioned before, the gravity can be ignored). Instead, the different asymmetries determine the propagation direction of the generated Lamb wave, causing the different rotation directions of the gold plate (more explanations are provided later).

[1]State Key Laboratory of Modern Optical Instrumentation, College of Optical Science and Engineering, Zhejiang University, Hangzhou 310027, China. [2]Department of Electrical and Computer Engineering, National University of Singapore, 4 Engineering Drive 3, Singapore 117583, Singapore. [3]School of Engineering, Westlake University, 18 Shilongshan Road, Hangzhou 310024, China. [4]Institute of Advanced Technology, Westlake Institute for Advanced Study, Westlake University, 18 Shilongshan Road, Hangzhou 310024, China.
*Corresponding author. Email: minqiu@zju.edu.cn, qiu_lab@westlake.edu.cn

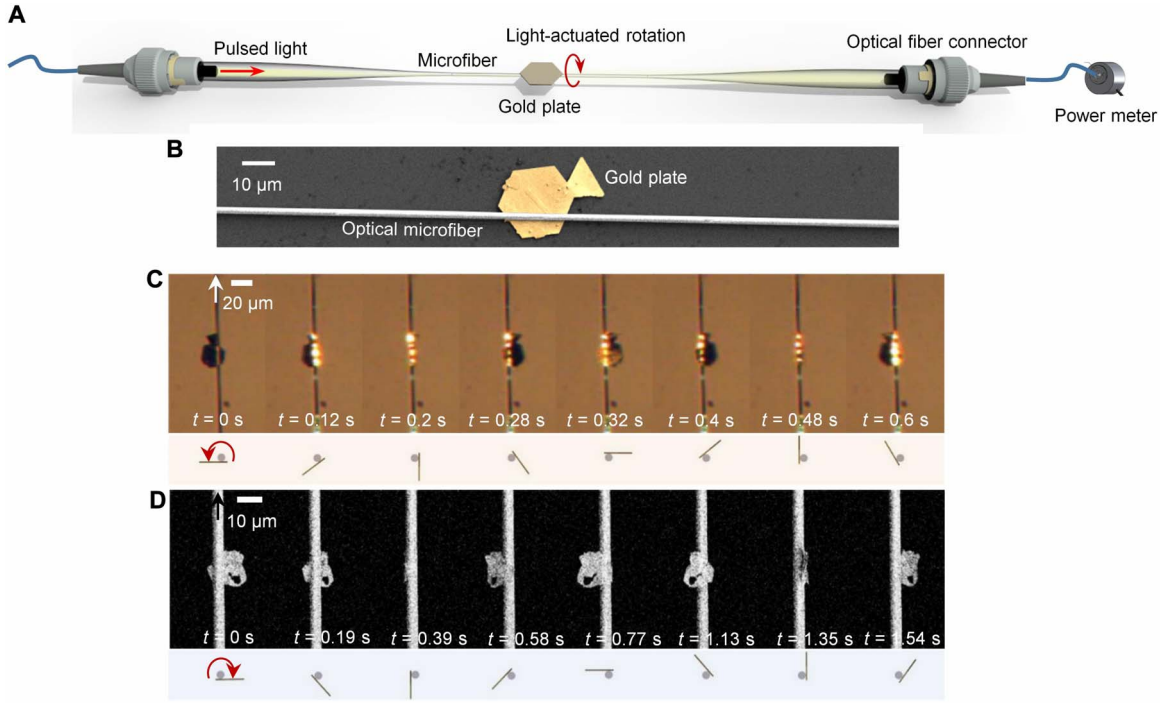

Fig. 1. Light-actuated rotation of a motor in air and vacuum. (**A**) Schematic of experimental configuration showing that a pulsed supercontinuum light (pulse duration, 2.6 ns; repetition rate, 5 kHz; wavelength, 450 to 2400 nm) is delivered into a microfiber and light power is measured by a power meter at the output end. The microfiber is suspended in air or vacuum, and the gold plate is placed on it and then rotates around it due to the actuation of the pulsed light. (**B**) False-color scanning electron micrograph of a gold plate (side length, 11 μm; thickness, 30 nm) below a microfiber with a radius of 880 nm. Note that the plate-microfiber system is placed on a silicon substrate after rotation experiments. (**C**) Sequencing optical microscopy images of the anticlockwise revolving gold plate around the microfiber in air (sample A, 5 kHz) (see movie S1). The measured average light power is 0.6 mW. (**D**) Sequencing SEM images of a clockwise revolving gold plate (long side length, 10.5 μm; short side length, 3.7 μm; thickness, 30 nm) around a microfiber (radius, 2 μm) in vacuum (see movie S2). The measured average light power is 1.5 mW. Arrows in (C) and (D) represent the direction of light propagation. Gray circles and yellow lines below (C) and (D) denote the microfiber and plate, respectively. Red curve arrows indicate the rotation direction of the plate.

The motor can work not only in air but also in vacuum, where the gas pressure is about nine orders of magnitude lower than that in air environment. Therefore, the impacts due to the photophoretic force, as one kind of commonly light-induced force (*18*), can be ruled out in vacuum (detailed discussion is provided in section S3). The experimental configuration of the motor system in vacuum is shown in fig. S2. Figure 1D shows a gold plate revolving around a microfiber in vacuum (see movie S2). The plate rotates at ~0.5 Hz clockwise.

The rotation speed of the motor is found linearly proportional to the repetition rate of light pulses, as shown in Fig. 2C (see also movies S1 and S6). The rotation speed of the plate can be gained from the period of effective width variation of the plate recorded in frames of experimental videos (Fig. 2A and fig. S6; see the definition of the effective width in fig. S5). It seems that the gold plate rotates around the microfiber continuously from the experimental videos. The gold plate, actuated by serial light pulses, rotates step by step, and the rotation is in the quasi-continuous regime. The power of every light pulse remains the same, and the repetition rate of the emitting light pulses increases. In this case, the rotation speed increases linearly, showing that a single light pulse can actuate the motor to rotate an extremely fine angle and the rotation angle for every light pulse remains almost constant independent of the repetition rate. This is further confirmed by the following experiments.

As mentioned above, every single light pulse actuates the motor to rotate a constant angle. On this basis, a desired rotation angle of the motor can be achieved if a specific number of light pulses are sent to the microfiber. We used a waveform generator to produce a triggering signal that can task the light source to emit a specific number of light pulses, as shown in Fig. 3A. The motor rotates step by step for the intermittent light pulse burst. The step angle increases linearly with the light pulse number, as shown in Fig. 3B. The motor rotates about 0.1° for every single light pulse. The step angle for every single light pulse can be smaller (e.g., 0.018°; see movie S4) if the power of the single light pulse decreases. However, if the power of the single light pulse is lower than the threshold, the motor will not work. Besides, if the power of the single light pulse is too high, the motor will be damaged due to high temperature. Stepping rotary motion of the motor actuated by the intermittent light pulse burst is shown in Fig. 3C (movie S3). The angle between the plate and the microfiber is calculated using the projection method (section S2).

A pulsed light source with a single wavelength (1064 nm) can also be used to drive the motor to rotate (movie S5). CW laser sources with different wavelengths (e.g., 532, 980, and 1064 nm) are used in experiments, but no rotation happens in these cases even when the laser power is high enough to melt the gold plate (thus, optical force can be ruled out as the driving force for the rotation; detailed discussion is provided in section S3). This further indicates that pulses play an essential role in generating motion of the motor. Pulsed light can excite coherent phonons and induce lattice expansion and contraction during the propagation of the acoustic wave (*19*). The pulsed light–induced

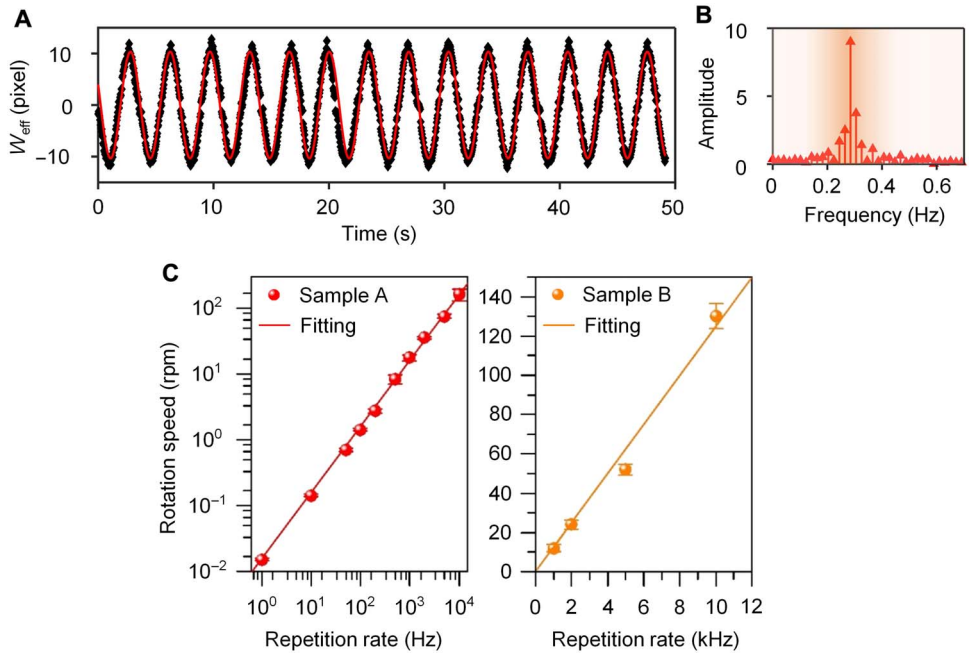

Fig. 2. Relationship between rotation speed and repetition rate. (**A**) Effective width (W_{eff}) of the plate obtained from every frame of experimental videos (sample A, 1 kHz). For convenience, the effective width of the plate is presented with pixel length (see also fig. S6). (**B**) Fourier transformation of the effective width to obtain its variation frequency (i.e., rotation speed of the plate). (**C**) Light-actuated rotation speed of the motor increases linearly with repetition rate of light pulses, and different samples give similar results (see movie S1 for sample A and movie S6 for sample B). The power for every light pulse remains the same when the repetition rate is changed. Error bars are the variance of rotation speed.

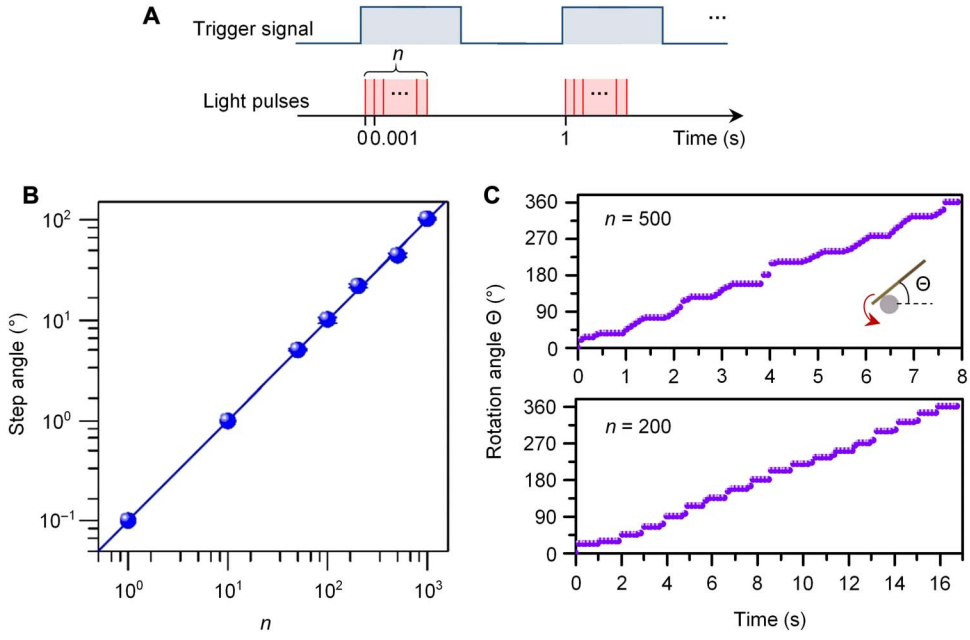

Fig. 3. A stepping rotary motor. (**A**) Schematic showing that a specific number (*n*) of light pulses are emitted at a 1-kHz repetition rate when the light source senses a positive edge on every trigger input. The 1-Hz electric trigger signal is generated by a waveform generator. (**B**) Step angle of the motor increasing linearly with the light pulse number (*n*) for one of the trigger inputs (see also movie S3). The motor rotates about 0.1° for every single light pulse. (**C**) Stepping rotation of the motor when the light pulse numbers (*n*) are 500 and 200.

acoustic wave has been used for many applications in optofluidics (*20*) and bioimaging (*21*). Besides, the surface acoustic wave (e.g., Rayleigh wave) can be generated on the surface of the light-absorbing film when the pulsed laser is focused as a line on the surface (*22*). Pulsed light absorbed by the film locally heats the film, leading to local thermo-elastic expansion and generation of the surface acoustic wave, which can be used for cleaning adhesive particles on surfaces (*23*). The electrically generated progressive surface acoustic wave can be used to drive a slider placed on the surface to move (*24*–*26*). When the thickness of a film or plate is smaller than the wavelength of a Rayleigh wave,

the Rayleigh wave will become a Lamb wave and the motion pattern of these two kinds of waves is very similar (*27*, *28*).

In our work, the pulsed light–induced Lamb wave, which is generated on the thin gold plate and acts on the surface of the microfiber, drives the plate to locomote on the microfiber surface. As shown in Fig. 4A, the pulsed light interacts with the gold plate in a line-shaped area through the evanescent field in the vicinity of the microfiber surface, which is analogous to a pulsed laser focused as a line on the gold plate using a cylindrical lens (*22*). Therefore, the generated Lamb wave mainly propagates in the direction perpendicular to the microfiber axis, resulting in rotation around the microfiber, instead of a translational motion along the microfiber axis. It can be considered that two Lamb waves are excited and propagate along the two sides of the gold plate with respect to the microfiber with the same initial amplitude. They are reflected back after reaching the boundary of the plate (figs. S8F and S10B). The asymmetric configuration of the plate on the microfiber results in unequal propagation length (i.e., unequal attenuation), and thus, the two Lamb waves cannot nullify their effect when they are reflected back from the edges of the plate. As a result, the Lamb wave (less attenuated) reflected from the shorter side of the plate dominates over the Lamb wave (more attenuated) reflected from the longer side. The result of these two waves propagates from the left to the right in the right-shifted case and from the right to the left in the left-shifted case (see Fig. 4, B and C).

To gain more insight into the mechanism of the pulsed light–generated Lamb wave in the asymmetrically configured thin plate, we carry out finite element–coupled thermal and elastic simulations (see numerical simulations of the Lamb wave in an asymmetrically configured plate in section S5). The simulation results confirm the propagation of the Lamb wave in the opposite direction for the two asymmetric configurations (figs. S8 and S9). The results also show that the propagation direction of the generated Lamb wave in this plate-microfiber system is independent of the direction of the light propagation in the microfiber. Additional experiments are performed to confirm that the different rotation direction of the plate is caused by the different asymmetric configuration of the plate on the microfiber (movie S10). First, we place the gold plate on the microfiber in the left-shifted case, and the plate rotates around the microfiber clockwise. Then, we rearrange the same plate on the same microfiber to the right-shifted case, which makes the plate to rotate anticlockwise. Besides, we reverse the direction of light propagation in the microfiber, and the rotation direction of the gold plate does not change (movie S10). Therefore, the rotation direction is independent of the light propagation direction and is only determined by the different asymmetric configuration of the plate on the microfiber. This is consistent with the characteristics of the propagation direction of the generated Lamb wave.

To understand the detailed mechanism of the Lamb wave–driven locomotion, we analyze the simulated results related to the generation of the Lamb wave. According to the characteristics of the Lamb wave (*27*), the neighboring atoms at individual positions of the gold plate surface expand/contract, forming an elliptical motion in a collective fashion. Figure 4 (B and C) illustrates a clockwise elliptical motion in the right-shifted case and an anticlockwise elliptical motion in the left-shifted case. It has a maximum horizontal velocity component at the ridges of the Lamb wave. This horizontal displacement direction is negative in the right-shifted case and positive in the left-shifted case. The displacement of gold atoms moves the gold plate in the same direction and opposite to the Lamb wave propagation. The related simulation results are provided in figs. S8 and S9. Note that the surface of the microfiber is curved, and the strong adhesion force in the radial direction

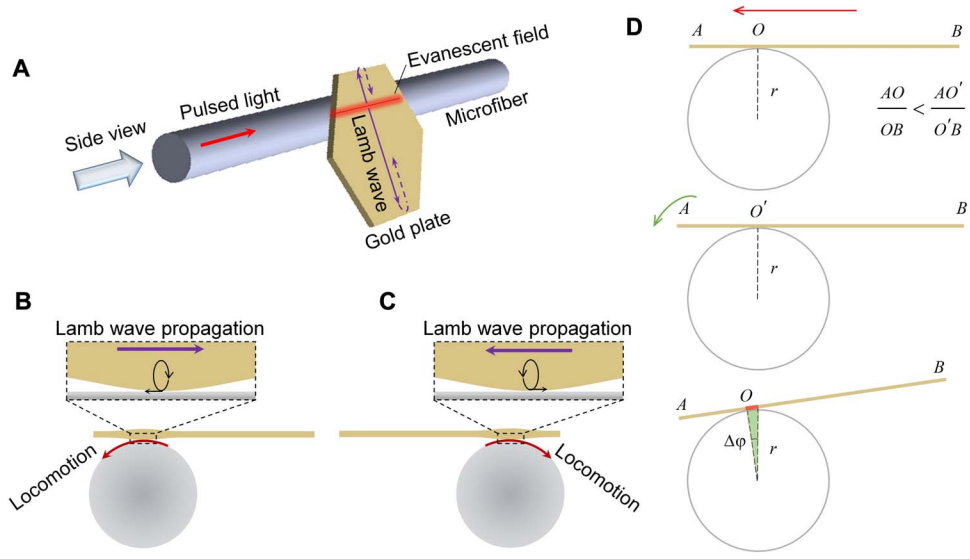

Fig. 4. Lamb wave–driven mechanism of the motor. (**A**) Schematic diagram showing a Lamb wave generated on the surface of a gold plate by line-shaped evanescent field outside a microfiber. (**B** and **C**) Schematic diagram (side view) showing (B) anticlockwise locomotion in the right-shifted case and (C) clockwise locomotion in the left-shifted case of the plate on the microfiber surface driven by the Lamb wave. Black ellipses in zoomed-in part represent collective motion pattern of surface gold atoms during the Lamb wave propagation. (**D**) Decomposition of movements showing synergic crawling and turning of the gold plate during one light pulse in the right-shifted case. Gray circle and yellow rectangle indicate the microfiber surface and plate, respectively. *A*, *B*, and *O* (*O*′) represent the head, end, and contact point of the plate, respectively. Note that the contact point represents the center point of the contact area. The plate crawls leftward (shown from top to middle), and the contact point of the plate changes from *O* to *O*′ ($\frac{AO}{OB} < \frac{AO'}{O'B}$). The plate turns at a slight angle (Δφ) (shown from middle to bottom). The plate locomotes a distance ($\Delta\varphi \cdot r$) after this series of movements, and the contact point of the plate remains unchanged.

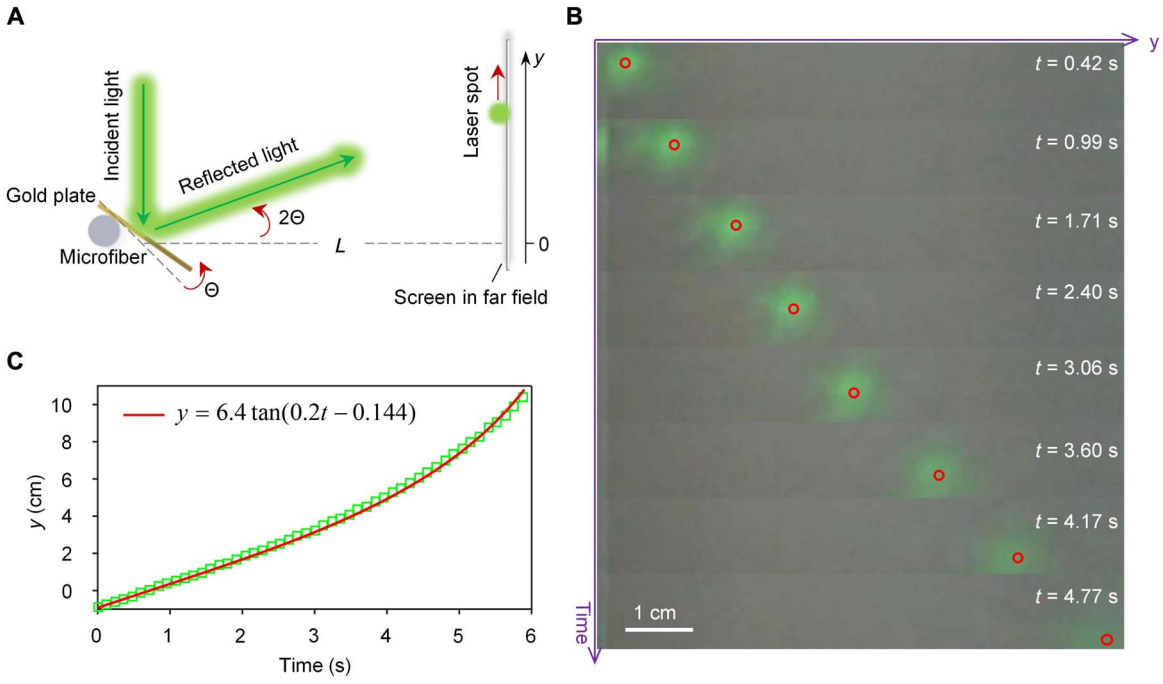

Fig. 5. One example application, demonstrating a micromirror for laser scanning. (**A**) Schematic representation of a rotary plate used as a micromirror to deflect the light beam. The reflected beam rotates 2θ when the plate rotates θ. The distance between the plate and the far field white screen is *L* (6.4 cm). The relationship between the position of the laser spot on the white screen (*y*) and the rotation angle of the reflected light (2θ) is $y = L \times \tan(2\theta)$. (**B**) Sequencing optical images of the laser spot (the center of which is marked with red circles) on the screen in the far field (see also movie S9). (**C**) Experimentally measured and theoretically expected position of the laser spot on the white screen. The rotational speed of the plate, actuated by light pulses at a repetition rate of 5 kHz in the experiment, is 0.95 rpm (0.1 rad/s). The preconceived relationship between *y* and *t* is $y = L \times \tan(2\omega t + \theta_0) = 6.4\tan(0.2t + \theta_0)$. θ_0 is the initial angle.

bends the plate naturally (fig. S1F), which makes the contact area larger and the contact tighter. The adhesion force in the radial direction centripetally pulls the gold plate to turn when it locomotes. Therefore, the gold plate, actuated by a series of light pulses, turns simultaneously while crawling upon the curvilinear microfiber step by step. Furthermore, the radial adhesion force enhances the interaction between the Lamb wave and the microfiber surface just as the assisted role of "preload" (*25*). As a result, the force that drives the plate to locomote forward is enlarged by the radial adhesion force.

Figure 4D elaborates the decomposition of the movements of the gold plate during actuation of one light pulse. The Lamb wave drives the gold plate to crawl leftward (from the top schematic to the middle schematic in Fig. 4D), and simultaneously, the radial adhesion force causes the gold plate to turn (from the middle schematic to the bottom schematic in Fig. 4D). As a result, the relative contact area on the gold plate, actuated by one pulse, remains unchanged after a small rotation. When the plate is actuated by a series of pulses, this synergetic coordination between crawling and turning ensures that the gold plate can rotate around the microfiber quasi-continuously and will not be detached from the microfiber (movie S8). The gold plate rotates a small angle Δφ, i.e., locomotes a distance $\Delta\varphi \cdot r$ after one-pulse actuation. For experimental results in movie S4, the rotation angle for one light pulse is 0.018° and the radius of the microfiber is 900 nm. Therefore, the locomotion distance for one light pulse (i.e., locomotion resolution) is 0.28 nm, which could be largely correlated with the vibration amplitude of the induced surface acoustic wave (see the theoretical model of locomotion resolution in section S4).

Our motor could be used as a micromirror to deflect the light beam, which is important for integrated optomechanics and outer-space applications in nonliquid environments. Pulsed light is guided into a microfiber and used to drive a plate to rotate. A 532-nm CW laser beam is focused on and reflected by the plate. A screen in the far field is used for displaying the projected laser spot (Fig. 5, fig. S7, and movie S9). The plate rotates anticlockwise, and the rotation angle for one light pulse (i.e., scanning resolution of this micromirror) is only about 0.001°. The reflected light rotates with double speed subsequently, and we can see that the projected laser spot moves upward in the far field screen. The measured position of the laser spot on the screen is in good agreement with the theoretical expectation (Fig. 5C).

DISCUSSION

We note that our motor is a light-actuated motor rotating around a fixed stator, which distinguishes it from previous mostly light-driven motors rotating around the center axis of itself (*7*–*13*). Our nanoscale motor can potentially be used in various fields, including prospective micro-opto-electromechanical systems in outer space, energy conversion, and vacuum high-precision mechanics. It can act as a micro-rotation stage in vacuum, the rotation axis of which is in the stage plane. By charging the metal plate, the rotating plate can possibly be used for radiating electromagnetic waves. As already demonstrated, the rotating plate could serve as a scanning micromirror to deflect a laser beam. The typical applications of this include laser scanning for miniature lidar systems (*29*) or laser display systems and optical modulating/switching for integrated microsystems. It could also function as a paddle for inducing gas motion in microfluidics systems. Furthermore, the discovery of this novel light-actuated locomotion phenomenon could open a new era of optical driving and manipulation, with subnanometer locomotion

resolution and controllable motion duration. It enables us to explore the new landscape of optical nanomanipulation in environments requiring a new paradigm for liquid-based manipulation.

MATERIALS AND METHODS

Microfiber fabrication and gold plate synthesis

Microfibers were fabricated using a flame-heated drawing technique (*30*). The fabrication procedures can be described as follows. A certain region of the coating layer of a single-mode optical fiber (standard communication fiber, Corning SMF-28e) was removed. The prefabricated fiber was put on a hydrogen flame torch, and the fiber was slowly pulled by the two motorized translation stages. The diameter of the microfiber, which was controlled by the pulling distance, ranged from several hundred nanometers to several micrometers. Gold plates were synthesized through an aniline-assisted (C_6H_7N) route in a mixture of ethylene glycol [$(CH_2OH)_2$] and chloroauric acid ($AuCl_3{\cdot}HCl{\cdot}4H_2O$), as reported previously (*31*). They are micrometer-sized single-crystalline gold plates (thickness, dozens of nanometers; size, several micrometers to a dozen micrometers). The shapes of these gold plates are mostly hexagons or triangles.

Experimental procedures

Two kinds of pulsed light sources were used in the experiments. One is a SuperK COMPACT supercontinuum laser (bandwidth, 450 to 2400 nm; pulse duration, 2.6 ns; repetition rate adjustable from 0.001 to 20 kHz; unpolarized). The other is a fixed-wavelength, Yb-doped, gain-switched fiber laser (wavelength, 1064 nm; pulse duration, 5 ns; repetition rate, 20 kHz; unpolarized). The synthesized gold plates were deposited on the glass substrate and then dried. A tapered fiber probe, which was manipulated by the three-dimensional console, was used to pick up a gold plate (fig. S1A) and to transfer the plate to a microfiber (fig. S1B). After experiments of light-actuated rotation, the gold plate was taken away from the microfiber to the substrate, as shown in fig. S1D for later experiments such as characterizations with SEM or atomic force microscopy (AFM). The experiments were first performed in air. An optical microscope was used for observation. The experiments were also performed in vacuum. In this case, the plate-microfiber system was put into the SEM chamber and the microfiber was connected to laser sources (outside the chamber) by an optical fiber through a vacuum connector, as shown in fig. S2.

SUPPLEMENTARY MATERIALS

Supplementary material for this article is available at http://advances.sciencemag.org/cgi/content/full/5/3/eaau8271/DC1

Section S1. Measurements of the adhesion force between gold plates and microfibers
Section S2. Extraction of the angle between gold plates and microfibers
Section S3. Ruling out the optical force and the photophoretic force as driving forces
Section S4. A theoretical model of locomotion resolution
Section S5. Numerical simulations of the Lamb wave in an asymmetrically configured plate
Fig. S1. Experimental procedures.
Fig. S2. Experimental configuration of the locomotor system in vacuum.
Fig. S3. Numerical calculation of plasmonic heating in the gold plate.
Fig. S4. Measurements of the adhesion force between gold plates and microfibers.
Fig. S5. Calculations of the angle between the gold plate and the microfiber using the projection method.
Fig. S6. Rotation of the locomotor actuated by light pulses with different repetition rates.
Fig. S7. Experimental system of a micromirror for optical sweeping.
Fig. S8. Numerical results of the Lamb wave generated in a gold plate.
Fig. S9. Wave motion patterns for the right-shifted and left-shifted asymmetric configurations.
Fig. S10. Lamb wave propagating in a larger gold plate.
Movie S1. A motor that is driven by a pulsed supercontinuum light with different repetition rates in air (sample A).
Movie S2. A motor that is driven by a pulsed supercontinuum light in vacuum.
Movie S3. A pulsed light–actuated stepping motor.
Movie S4. A lower power of the light pulse and a smaller rotation step for the locomotor.
Movie S5. A motor that is driven by a 1064-nm pulsed light in air.
Movie S6. A motor that is driven by a pulsed supercontinuum light with different repetition rates in air (sample B).
Movie S7. Deforming the microfiber to measure the adhesion force.
Movie S8. An animation to illustrate the rotary locomotion of the motor.
Movie S9. A light-actuated rotary micromirror.
Movie S10. Rotation direction of the motor controlled by different asymmetric configurations.
References (*32*–*41*)

REFERENCES AND NOTES

1. O. Lehmann, M. Stuke, Laser-driven movement of three-dimensional microstructures generated by laser rapid prototyping. *Science* **270**, 1644–1646 (1995).
2. A. M. Fennimore, T. D. Yuzvinsky, W. Q. Han, M. S. Fuhrer, J. Cumings, A. Zettl, Rotational actuators based on carbon nanotubes. *Nature* **424**, 408–410 (2003).
3. S. Sundararajan, P. E. Lammert, A. W. Zudans, V. H. Crespi, A. Sen, Catalytic motors for transport of colloidal cargo. *Nano Lett.* **8**, 1271–1276 (2008).
4. J. Wang, Cargo-towing synthetic nanomachines: Towards active transport in microchip devices. *Lab Chip* **12**, 1944–1950 (2012).
5. R. M. Berry, H. C. Berg, Absence of a barrier to backwards rotation of the bacterial flagellar motor demonstrated with optical tweezers. *Proc. Natl. Acad. Sci. U.S.A.* **94**, 14433–14437 (1997).
6. Z. Bryant, M. D. Stone, J. Gore, S. B. Smith, N. R. Cozzarelli, C. Bustamante, Structural transitions and elasticity from torque measurements on DNA. *Nature* **424**, 338–341 (2003).
7. K. Kim, J. Guo, Z. X. Liang, F. Q. Zhu, D. L. Fan, Man-made rotary nanomotors: A review of recent developments. *Nanoscale* **8**, 10471–10490 (2016).
8. S. Maruo, A. Takaura, Y. Saito, Optically driven micropump with a twin spiral microrotor. *Opt. Express* **17**, 18525–18532 (2009).
9. S. L. Neale, M. P. MacDonald, K. Dholakia, T. F. Krauss, All-optical control of microfluidic components using form birefringence. *Nat. Mater.* **4**, 530–533 (2005).
10. N. B. Simpson, K. Dholakia, L. Allen, M. J. Padgett, Mechanical equivalence of spin and orbital angular momentum of light: An optical spanner. *Opt. Lett.* **22**, 52–54 (1997).
11. M. Liu, T. Zentgraf, Y. Liu, G. Bartal, X. Zhang, Light-driven nanoscale plasmonic motors. *Nat. Nanotechnol.* **5**, 570–573 (2010).
12. P. Němec, E. Rozkotová, N. Tesařová, F. Trojánek, E. De Ranieri, K. Olejník, J. Zemen, V. Novák, M. Cukr, P. Malý, T. Jungwirth, Experimental observation of the optical spin transfer torque. *Nat. Phys.* **8**, 411–415 (2012).
13. D. Hakobyan, E. Brasselet, Left-handed optical radiation torque. *Nat. Photon.* **8**, 610–614 (2014).
14. R. A. Bowling, A theoretical review of particle adhesion, in *Particles on Surfaces 1*, K. L. Mittal, Ed. (Springer, 1988), pp. 129–142.
15. R. A. Freitas Jr., Nanotechnology, nanomedicine and nanosurgery. *Int. J. Surg.* **3**, 243–246 (2005).
16. D. Gao, W. Ding, M. Nieto-Vesperinas, X. Ding, M. Rahman, T. Zhang, C. Lim, C.-W. Qiu, Optical manipulation from the microscale to the nanoscale: Fundamentals, advances and prospects. *Light Sci. Appl.* **6**, e17039 (2017).
17. J. Lu, Y. Hong, Q. Li, Y. Xu, W. Fang, M. Qiu, Light-induced reversible expansion of individual gold nanoplates. *AIP Adv.* **7**, 105025 (2017).
18. J. Lu, H. Yang, L. Zhou, Y. Yang, S. Luo, Q. Li, M. Qiu, Light-induced pulling and pushing by the synergic effect of optical force and photophoretic force. *Phys. Rev. Lett.* **118**, 043601 (2017).
19. J. Chen, W. K. Chen, J. Tang, P. M. Rentzepis, Time-resolved structural dynamics of thin metal films heated with femtosecond optical pulses. *Proc. Natl. Acad. Sci. U.S.A.* **108**, 18887–18892 (2011).
20. Y. Wang, Q. Zhang, Z. Zhu, F. Lin, J. Deng, G. Ku, S. Dong, S. Song, M. K. Alam, D. Liu, Z. Wang, J. Bao, Laser streaming: Turning a laser beam into a flow of liquid. *Sci. Adv.* **3**, e1700555 (2017).
21. H. F. Zhang, K. Maslov, G. Stoica, L. V. Wang, Functional photoacoustic microscopy for high-resolution and noninvasive in vivo imaging. *Nat. Biotechnol.* **24**, 848–851 (2006).
22. P. Hess, A. M. Lomonosov, A. P. Mayer, Laser-based linear and nonlinear guided elastic waves at surfaces (2D) and wedges (1D). *Ultrasonics* **54**, 39–55 (2014).
23. A. A. Kolomenskii, H. A. Schuessler, V. G. Mikhalevich, A. A. Maznev, Interaction of laser-generated surface acoustic pulses with fine particles: Surface cleaning and adhesion studies. *J. Appl. Phys.* **84**, 2404–2410 (1998).
24. R. M. Moroney, R. M. White, R. T. Howe, Ultrasonic micromotors, in *IEEE Ultrasonics Symposium Proceedings* (IEEE, 1989).

25. M. K. Kurosawa, M. Takahashi, T. Higuchi, Elastic contact conditions to optimize friction drive of surface acoustic wave motor. *IEEE Trans. Ultrason. Ferroelectr. Freq. Control* **45**, 1229–1237 (1998).
26. T. Shigematsu, M. K. Kurosawa, K. Asai, Nanometer stepping drives of surface acoustic wave motor. *IEEE Trans. Ultrason. Ferroelectr. Freq. Control* **50**, 376–385 (2003).
27. H. Lamb, On waves in an elastic plate. *Proc. R. Soc. Lond. Ser. A* **93**, 114–128 (1917).
28. L. Rayleigh, On waves propagated along the plane surface of an elastic solid. *Proc. Lond. Math. Soc.* **1**, 4–11 (1885).
29. B. Schwarz, Mapping the world in 3D. *Nat. Photonics* **4**, 429–430 (2010).
30. Y. Xu, W. Fang, L. Tong, Real-time control of micro/nanofiber waist diameter with ultrahigh accuracy and precision. *Opt. Express* **25**, 10434–10440 (2017).
31. Z. Guo, Y. Zhang, Y. DuanMu, L. Xu, S. Xie, N. Gu, Facile synthesis of micrometer-sized gold nanoplates through an aniline-assisted route in ethylene glycol solution. *Colloids Surf. A* **278**, 33–38 (2006).
32. R. P. Feynman, R. B. Leighton, M. Sands, Elasticity, in *The Feynman Lectures on Physics* (Addison Wesley Longman, 1970), vol. 2, ch. 38.
33. H. C. Hamaker, The London-van der Waals attraction between spherical particles. *Physica* **4**, 1058–1072 (1937).
34. Y. I. Yalamov, V. B. Kutukov, E. R. Shchukin, Theory of the photophoretic motion of the large-size volatile aerosol particle. *J. Colloid Interf. Sci.* **57**, 564–571 (1976).
35. M. Scandurra, F. Iacopetti, P. Colona, Gas kinetic forces on thin plates in the presence of thermal gradients. *Phys. Rev. E* **75**, 026308 (2007).
36. K. Wang, E. Schonbrun, K. B. Crozier, Propulsion of gold nanoparticles with surface plasmon polaritons: Evidence of enhanced optical force from near-field coupling between gold particle and gold film. *Nano Lett.* **9**, 2623–2629 (2009).
37. X. Chen, Y. T. Chen, M. Yan, M. Qiu, Nanosecond photothermal effects in plasmonic nanostructures. *ACS Nano* **6**, 2550–2557 (2012).
38. A. J. Schmidt, R. Cheaito, M. Chiesa, Characterization of thin metal films via frequency-domain thermoreflectance. *J. Appl. Phys.* **107**, 024908 (2010).
39. D. A. Hutchins, K. Lundgren, S. B. Palmer, A laser study of transient Lamb waves in thin materials. *J. Acoust. Soc. Am.* **85**, 1441–1448 (1989).
40. C. Rossignol, J. M. Rampnoux, M. Perton, B. Audoin, S. Dilhaire, Generation and detection of shear acoustic waves in metal submicrometric films with ultrashort laser pulses. *Phys. Rev. Lett.* **94**, 166106 (2005).
41. S. Maier, *Plasmonics: Fundamentals and Applications* (Springer, 2007).

Acknowledgments: We thank Y. X. Xu, N. Yao, and W. Fang (Zhejiang University) for their help in fabricatng the microfiber. We are also grateful to T. H. Zhang (National University of Singapore) and L. Meng (Zhejiang University) for their assistance and valuable inputs. **Funding:** This project was supported by the National Key Research and Development Program of China (grant nos. 2017YFA0205700 and 2017YFE0100200 to M.Q. and Q.L.), the National Natural Science Foundation of China (grant nos. 61425023, 61575177, and 61775194 to M.Q. and Q.L.), and the Ministry of Education, Singapore (grant no. R-263-000-D11-114 to C.-W.Q.). **Author contributions:** J.L. and M.Q. conceived the idea and designed the experiments. M.Q. supervised the overall research together with Q.L. J.L. performed the experiments and simulations. J.L., M.Q., C.-W.Q., P.G., and Y.H. analyzed the results. All the authors contributed to the final manuscript. **Competing interests:** The authors declare that they have no competing interests. **Data and materials availability:** All data needed to evaluate the conclusions in the paper are present in the paper and/or the Supplementary Materials. Additional data related to this paper may be requested from the authors.

Submitted 18 July 2018
Accepted 23 January 2019
Published 8 March 2019
10.1126/sciadv.aau8271

Citation: J. Lu, Q. Li, C.-W. Qiu, Y. Hong, P. Ghosh, M. Qiu, Nanoscale Lamb wave–driven motors in nonliquid environments. *Sci. Adv.* **5**, eaau8271 (2019).

Science Advances

Nanoscale Lamb wave–driven motors in nonliquid environments

Jinsheng Lu, Qiang Li, Cheng-Wei Qiu, Yu Hong, Pintu Ghosh and Min Qiu

Sci Adv **5** (3), eaau8271.
DOI: 10.1126/sciadv.aau8271